A Comparative Study of Instabilities in Forced Reacting Plumes of Nonpremixed Flames

Jieyu Jiang [a], Liyue Jing [b], Min Zhu [b], Xi Jiang [c *]

[a] State Key Laboratory of Fire Science, University of Science and Technology of China, Hefei, Anhui 230026, China

[b] Department of Thermal Engineering, Tsinghua University, Beijing 100084, China

[c] Engineering Department, Lancaster University, Lancaster LA1 4YR, United Kingdom

[*] Corresponding author. E-mail: x.jiang@lancaster.ac.uk; Tel: (+44) 1524 592439

Highlights:

- The flow instabilities of nonpremixed methane-air flames are investigated.
- The experimental, numerical and theoretical studies show qualitative agreements.
- The flow convective instability is coupled with buoyancy-driven instability.
- The nonpremixed flame system exhibits a low-pass characteristic.

Abstract

A comparative study has been performed to investigate the flow instabilities and their interaction for nonpremixed methane-air flames using experimental results, numerical simulations and theoretical analyses. The effects of buoyancy and the strong external perturbations on the vortex dynamics and instabilities of forced reacting plumes are studied. Results suggest that the flame surface breaks in forced reacting plumes and two flame fronts are formed eventually due to the convective instability coupled with buoyancy-driven instability. Flame pinch-off could occur in a short time for the cases with the strong perturbations of low frequencies. This indicates that the nonpremixed flame system exhibits a low-pass characteristic, which is sensitive to the low frequency perturbations. In addition, the buoyancy instability can be observed from the comparisons, which is of an absolute unstable nature. Despite the fact that theoretical analyses are derived from the single transport equation for mixture fraction with a

number of assumptions, the results are still in good agreement with those obtained from the experiments and numerical simulations.

Key words: Plumes; Flame instability; Vortical structure; Low-pass characteristic

1 Introduction

Nonpremixed flames have been studied for decades by many researchers since they are relevant to many practical applications, such as jet engines, rockets, and industry furnaces. The combustion instability of nonpremixed flames is not only an important academic research topic but also crucial to the system safety in industrial applications. Jet diffusion flames may subject to various instabilities, including hydrodynamic instability, buoyancy-driven instability and acoustic instability.

The jet shear layer of burnt gases has an inflexional velocity profile and is unstable in the sense of Kelvin-Helmholtz instability. It is a kind of hydrodynamic instability, which can be either an absolute instability or a convective instability (Huerre and Monkewitz, 1985). The increasing of fuel jet flow rate may lead to the formation of vortical structures inside the flame surface, and flow transition to turbulence in the reacting flow (Savas and Gollahalli, 1986; Lieuwen, 2012).

Buoyancy-driven instability has been studied by numerical, theoretical and experimental investigations respectively. For example, buoyancy could cause the flame front to oscillate or flicker regularly at a low frequency, typically ranging from 10 to 20 Hz (Buckmaster and Peters, 1988). Lower flickering frequencies were also reported, e.g. Wang et al. (2013) reported a natural frequency of 7.8 Hz. For predicting the buoyancy-induced flame flickering frequency, Gotoda et al. (2007) investigated a rotating Bunsen burner under the swirling flow conditions by experiment, focusing on how the flame flickering frequency changed with increasing swirl numbers. Buoyancy could cause vortical structures outside the flame surface (Eickhoff, 1982; Roquemore et al., 1989; Katta et al., 1994). The evolution of vortical structures in buoyant thermal

plumes, their interaction with flames and the low frequency oscillations have also been studied extensively, e.g. Chamberlin and Rose (1928), Yule et al. (1981) and Wang et al. (2012).

The existence of vortical structures inside and outside the flame surface was a characteristic of transitional jet diffusion flames (Goss et al., 1994). Grout et al. (2012) investigated the flame structure of a transverse jet in a cross-flow of air. Doom and Mahesh (2009) showed that the fuel rich reacting vortex ring provided the highest temperature in the flow field, while the fuel lean reacting vortex ring had little effect on the flow, and this was similar to a non-reacting vortex ring.

Hydrodynamic instabilities including buoyancy-driven instability are commonly encountered in reacting flows. In practical applications, combustion instability may occur when the combustion process has an interaction with other system components, such as acoustic instability. In rockets and gas turbines, the unsteady combustion can cause acoustic oscillations and then respond to the reflected acoustic waves. The response of nonpremixed flames to flow perturbations was investigated theoretically, e.g. Tyagi et al. (2007), Balasubramanian and Sujith (2008) and Magina et al. (2013). For industrial applications, the distributed flame transfer function of nonpremixed flames was obtained by the low-order model analysis (Yao and Zhu, 2012; Zhu et al., 2005).

Different combustion instabilities can couple with each other in industrial applications and make the problem more complex. This topic becomes increasingly important and has received lots of attentions in recent years. Jiang and Luo (2000a) studied the dynamic behaviors of reacting plumes using direct numerical simulation. The buoyancy-driven flows displayed a naturally developed instability which did not depend on external small-amplitude perturbations. Juniper et al. (2009) carried out an experimental and numerical study of self-excited round jet diffusion flames under acoustic forcing and investigated the lock-in and quasi-periodicity phenomena. Many attempts have been made to investigate the flame instabilities, however, there are still a lack of a detailed understanding on the interaction of different kinds of instabilities and their corresponding effects. Therefore the complex problem for combustion instabilities needs further investigations. In this study, a combined approach of experiments,

theoretical analyses and numerical simulations with their respective advantages to complement each other is adopted to study the flame surface and vortical structures under different flow instabilities.

The main motivation of this study is to further investigate different kinds of instabilities and their interaction for nonpremixed flames. The generation and evolution of vortical structures are investigated, aiming at understanding the influence of different instabilities in practical combustion applications. Particular attention has been given to the effects of buoyancy and different strong external perturbations on the vortex dynamics and locations of the surfaces of nonpremixed flames. The combined approach may provide a deeper physical insight by more easily identifying cause and effect.

2 Experimental, theoretical and computational approaches

In this study, experimental, theoretical and computational approaches are employed to investigate the instabilities in forced reacting plumes of nonpremixed flames. The methodologies used are briefly explained as follows.

2.1 Experimental facilities

The physical problem is a gaseous methane jet issuing into an air coflow. As shown in Fig. 1, the nonpremixed methane-air experimental combustion system contains combustor, optical system, control system and data acquisition (DAQ) system, etc. The schematic diagram of the nonpremixed methane-air coflow burner and its sizes are illustrated in Fig. 2. Fuel and air are separately injected into the burner and controlled by the flow volume controllers. The initial velocity of methane at the nozzle exit is 0.558 m/s, and the air coflow velocity is 0.205 m/s. The inner and outer diameters of the fuel pipe are 4.50 mm and 6.84 mm respectively, which is located concentrically in the air pipe with an inner diameter of 44 mm. The strong external perturbations are imposed on the air coflow by two loudspeakers in order to trigger the unstable mode of flames. Two-microphone method is used to measure air velocity fluctuations at the outlet of the burner. The forced amplitude A of external perturbations is defined as the amplitude of

velocity perturbation normalized by the bulk jet velocity ($A \equiv \left| u_0^{'} \right| / \overline{u}_0$), which was chosen as 0.5 in the experimental measurements. This large amplitude of perturbation was chosen to clearly identify the response of the nonpremixed flames to external forcing. In the experiments, the forced frequencies were selected as 20 Hz, 30 Hz, and 40 Hz respectively.

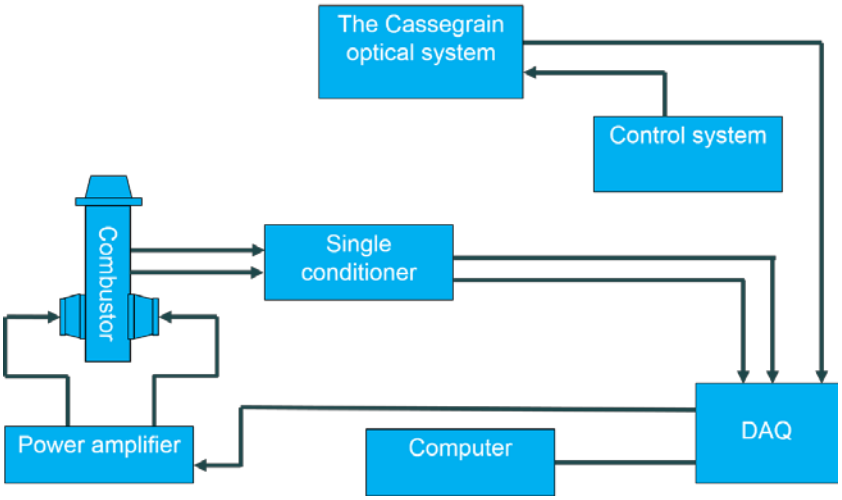

Fig. 1 The schematic diagram of the nonpremixed flame experimental system

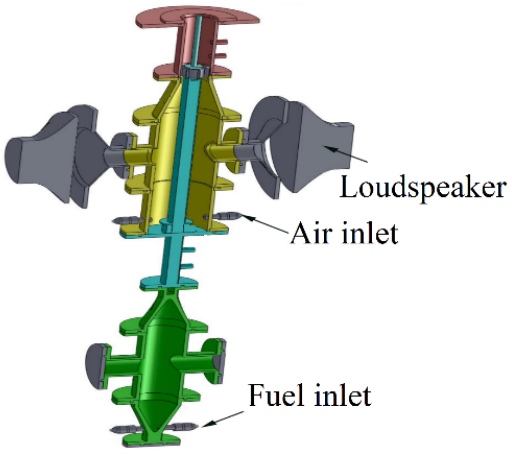

(a)

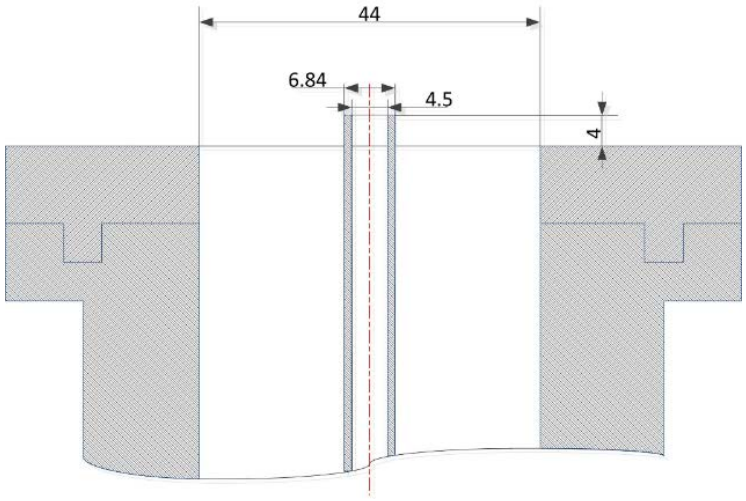

(b)

Fig. 2 The schematic diagram of nonpremixed methane-air coflow burner (a) and its sizes (b) (unit: mm)

2.2 Computational method

2.2.1 Governing equations

Numerical simulations are performed for the combustion system based on the experimental facilities. In this study, five cases of direct numerical simulations for the nonpremixed methane-air flames are performed for comparison, which can isolate the buoyancy effect from the instability induced by external perturbations to complement the results obtained from the experiments. Since the study is focused on the near-field instabilities of diffusion flames, two-dimensional axisymmetric simulations which can avoid the excessively high computational costs of fully three-dimensional simulations are considered to be sufficient.

As shown in Fig. 3, the reacting flow field above the jet nozzle plane is solved in the axisymmetric cylindrical coordinates and described by the following compressible Navier-Stokes equations. The original dimensional form of conservation equations are written as:

Mass conservation:

$$\frac{\partial \rho^*}{\partial t^*} = -\nabla_j \cdot \left(\rho^* \mathbf{u}_j^* \right), \tag{1}$$

Momentum conservation:

$$\frac{\partial(\rho^*\mathbf{u}_j^*)}{\partial t^*} = -\nabla_k \cdot (\rho^*\mathbf{u}_j^*\mathbf{u}_k^*) + \nabla_k \cdot \tau_{jk}^* - \nabla_j \cdot p^* + \rho^*\mathbf{g}_j^*, \tag{2}$$

Energy conservation:

$$\frac{\partial\left(\rho^* e^*\right)}{\partial t^*} = -\nabla_k \cdot [(\rho^* e^* + p^*)\mathbf{u}_k^*] - \nabla_k \cdot \mathbf{q}_k^* + \nabla_k \cdot (\mathbf{u}_j^*\tau_{jk}^*) + \rho^*\mathbf{g}_k^*\mathbf{u}_k^*, \tag{3}$$

Transport equations for species

$$\frac{\partial(\rho^* Y_i^*)}{\partial t^*} = -\nabla_k \cdot (\rho^*\mathbf{u}_k^* Y_i^*) + \nabla_k \cdot (\rho^* D_i^* \frac{\partial Y_i^*}{\partial x_k^*}) + \omega_Y^*, \tag{4}$$

The equation of state

$$p^* = \rho^* R^* T^*. \tag{5}$$

where ρ^*, t^*, u_j^*, e^*, p^*, Y_i^* stand for density, time, velocity components in the x_j direction, total energy per unit mass, pressure, the mass fraction of species *i* respectively. Here the superscript * stands for dimensional quantities. Viscous effects are represented by stress tensor τ^*, and the constitutive relationship of stress tensor is given by

$$\tau_{jk}^* = \mu^*\left(\nabla_j \mathbf{u}^*{}_k + \nabla_k \mathbf{u}^*{}_j - \frac{2}{3}\delta_{jk}\nabla_i \mathbf{u}^*{}_i\right) \tag{6}$$

Neglecting the differential diffusion of species and DuFour effects, the heat flux components are given as $\boldsymbol{q}_k^* = -\lambda^* \nabla_k \cdot T^*$, and diffusion coefficients $\rho^* D_i^*$ for every species are given by $\rho^* D_i^* = \lambda^* / C_P^*$ with the unity Lewis number assumption. The reaction rate ω_Y^* is calculated by a simple reaction $CH_4 + 2O_2 \rightarrow CO_2 + 2H_2O$, which is presumed for the methane-air flames to facilitate the study by avoiding the prohibitive computational cost involving complex chemistry. Finite-rate chemistry described by the Arrhenius law is adopted for the calculation of ω_Y^* (Jiang and Luo, 2000b).

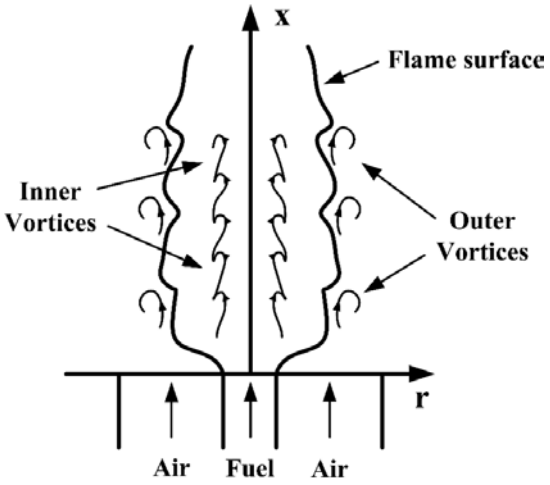

Fig. 3 Sketch of the axisymmetric nonpremixed jet flame

With reference to properties in the fuel stream at the inflow including the jet nozzle diameter l_0^*, fuel velocity u_{f0}^* and the ambient temperature T_0^*, the non-dimensional form of governing equations is employed. In addition, the reference quantities ρ_0^*, μ_0^*, λ_0^*, C_{p0}^* represent the fuel density, viscosity, thermal conductivity, specific heat at constant pressure at ambient temperature respectively, and $g_0^* = 9.81\ \mathrm{ms}^{-2}$. Consequently, the conservation laws for mass, momentum, energy and chemical species can be written in the non-dimensional form as

$$\frac{\partial \mathbf{Q}}{\partial t} + \frac{\partial \mathbf{F}}{\partial x} + \frac{1}{r}\frac{\partial (\mathbf{G}r)}{\partial r} + \mathbf{S}_\mathbf{r} = 0 \qquad (7)$$

where the vectors **Q**, **F**, **G** and $\mathbf{S}_\mathbf{r}$ are defined as

$$\mathbf{Q}=\begin{pmatrix}\rho\\ \rho u\\ \rho v\\ \rho e\\ \rho Y_i\end{pmatrix},\quad \mathbf{S_r}=\begin{pmatrix}0\\ -\rho g/Fr\\ (-p+\tau_{\theta\theta})/r\\ -\rho ug/Fr+q_h\\ w_Y\end{pmatrix},$$

$$\mathbf{F}=\begin{pmatrix}\rho u\\ \rho u^2+\mathrm{p}-\tau_{xx}\\ \rho uv-\tau_{xr}\\ (\rho e+p)u+q_x-u\tau_{xx}-v\tau_{xr}\\ \rho uY_i-\dfrac{1}{\mathrm{Re}\,Sc}\left(\dfrac{\lambda}{C_p}\dfrac{\partial Y_i}{\partial x}\right)\end{pmatrix},$$

$$\mathbf{G}=\begin{pmatrix}\rho v\\ \rho uv-\tau_{xr}\\ \rho v^2+p-\tau_{rr}\\ (\rho e+p)v+q_r-v\tau_{rr}-u\tau_{xr}\\ \rho vY_i-\dfrac{1}{\mathrm{Re}\,Sc}\left(\dfrac{\lambda}{C_p}\dfrac{\partial Y_i}{\partial r}\right)\end{pmatrix}.$$

The non-dimensional equation of state is also rewritten as $p=\dfrac{\rho T}{\gamma M^2}$. Here the non-dimensional numbers such as Mach number *M*, Froude number *Fr*, Reynolds number *Re* and Schmidt number *Sc* are calculated from $M=\dfrac{u_0^*}{\sqrt{\gamma R_0^* T_0^*}}$, $Fr=\dfrac{u_0^{*2}}{g_0^* l_0^*}$, $Re=\dfrac{\rho_0^* u_0^* l_0^*}{\mu_0^*}$ and $Sc=\dfrac{\mu_0^* C_{P0}^*}{\lambda_0^*}$ respectively. However, at the centerline, a new set of equations are used to circumvent the singularity in the mathematical formulation by applying L'Hospital's rule. Therefore the special conversation laws at $r = 0$ are described as

$$\frac{\partial \mathbf{Q}}{\partial t}+\frac{\partial \mathbf{F}}{\partial x}+\frac{\partial \mathbf{G}}{\partial r}+\frac{\partial \mathbf{H}}{\partial r}+\mathbf{S}_r'=0 \qquad (8)$$

where the vectors **H** and $\mathbf{S}_\mathbf{r}'$ are given as

$$\mathbf{H}=\begin{pmatrix} \rho v \\ \rho uv-\tau_{xr} \\ \rho v^2+p-\tau_{rr} \\ (\rho e+p)v+q_r-v\tau_{rr}-u\tau_{xr} \\ \rho vY_i-\dfrac{1}{\mathrm{Re}\,Sc}\left(\dfrac{\lambda}{C_p}\dfrac{\partial Y_i}{\partial r}\right) \end{pmatrix},$$

$$\mathbf{S}'_r=\begin{pmatrix} 0 \\ -\rho g/Fr \\ 0 \\ -\rho ug/Fr+q_h \\ w_Y \end{pmatrix}$$

2.2.2 Numerical methods

The reacting flow field above the jet nozzle plane is solved by the above non-dimensional governing equations for the axisymmetric configuration. The spatial differentiation of these equations is performed using a sixth-order accurate compact finite difference scheme for evaluation of the spatial derivatives (Lele, 1992). A third-order fully explicit compact-storage Runge-Kutta scheme (Williamson, 1980) is used to advance the equations in time. The time step is limited by the Courant-Friedrichs-Lewy condition number for stability and a chemical restraint, and an increase in the local product mass fraction of more than 0.01% is not allowed for one time step (Jiang and Luo, 2000b).

The jet nozzle exit is taken as an inflow boundary, while the further downstream of the jet is assumed to be an outflow boundary. The inflow is specified using the Navier-Stokes characteristic boundary conditions (Poinsot and Lele, 1992), with temperature treated as a “soft” variable, which is calculated during the simulation rather than fixed and allowed to fluctuate according to the characteristic waves at the boundary. Non-reflecting characteristic boundary condition is used for the outflow boundary. Because the flow is not necessarily going out of the domain instantaneously in the direction normal to the outflow boundary due to the existence of multidimensional vortical structures, a sponge layer is applied next to the boundary to control spurious

wave reflections. At the lateral boundaries, the normal velocity is calculated from the characteristic momentum equation by applying the local one-dimensional inviscid relations, which allows the flow entrainment without causing numerical wave reflections. Further extending the size of the domain in the lateral direction did not lead to appreciable changes in the flow solution.

The axisymmetric buoyant plumes originating from a 4.5 mm diameter nozzle are forced in a periodic manner by two loudspeakers. For the fuel jet and air coflow at the inlet, a "top-hat" velocity profile is specified for the streamwise velocity,

$$u(r)=\frac{u_{f0}}{2}\left\{1-tanh\left[\frac{0.5}{4\delta}\left(\frac{r}{0.5}-\frac{0.5}{r}\right)\right]\right\}+\frac{u_{a0}}{2}\left\{1-tanh\left[\frac{0.5}{4\delta}\left(\frac{r}{0.5}-\frac{0.5}{r}\right)\right]\right\} \quad (9)$$

where u_{f0} and u_{a0} stand for the non-dimensional initial velocities of fuel and air in the experiment, 0.5 represents the non-dimensional jet nozzle radius and δ stands for momentum thickness, which is chosen to be 10% of jet radius. In the simulations, the streamwise velocity is initialized with the above profile, while the radial velocity is taken as zero. A sinusoidal streamwise velocity oscillation at the nozzle exit is introduced as follows.

$$u'=Asin\left(2\pi f_0 t\right) \quad (10)$$

Here the amplitude A and frequency f_0 of velocity perturbations are dependent on the values selected in experiments. The methane jet at the nozzle exit is subject to a high temperature with a non-dimensional value of 4.0, which is chosen to ensure auto-ignition when fuel and air mix with each other. The results of simulations presented here are obtained from a grid with 901×400 points, which was found to be able to produce grid-independent results.

2.3 Theoretical analyses

In theoretical approaches, assumptions to simplify the problem are necessary in order to obtain solutions of the flow equations. Considering the classical Burke-Schumann diffusion flames, the flow field assumptions are given as follows. The incompressible flow moves at a low speed in x direction and the velocity field is

assumed to be homogenous and constant. The density and pressure of the flow field and the coefficient of diffusion for chemical species are all constants. The process of combustion described by the infinitely fast reaction depends on the diffusion of fuel and oxidizer and is confined to a thin reaction sheet where the mixture is stoichiometric. Accordingly the nonpremixed flames can be described by the following non-dimensional transport equation for mixture fraction Z with assumptions similar to those of Burke and Schumann flames to simplify the expressions.

$$\frac{\partial Z}{\partial t}+u\frac{\partial Z}{\partial x}=\frac{1}{Pe}\left(\frac{\partial^2 Z}{\partial x^2}+\frac{\partial^2 Z}{\partial y^2}\right) \tag{11}$$

Here the non-dimensional Peclet number is expressed as $Pe = u_{a0}^{*}\, l_0^{*} / D^{*}$, and D^{*} is the diffusion coefficient of fuel and air. With the assumption of a point source for the fuel slot, the line-source solution for the finite width fuel slot can be derived by integrating the point-source solution. With suitable boundary and initial conditions, the solution of Eq. (11) can be written in an explicit form with Green's function method. Considering the wall bounding effect with the image method (Carpio et al., 2012; Cumpsty and Marble, 1977), the non-dimensional transport equation for mixture fraction is solved for an instantaneous point source of unit release at the point x = 0, y = 0 (Stakgold and Holst, 2011; Poinsot and Veynante, 2005), which is described as

$$S_Z\left(x,y,t\right)=\sum_{n=-\infty}^{\infty}\frac{Pe}{4\pi t}\left\{\exp-\left[\frac{Pe\left(x-ut\right)^2}{4t}+\frac{Pe\left(y-2nL\right)^2}{4t}\right]\right\} \tag{12}$$

Eq. (12) is obtained by the superposition of solutions from the source at $Z_{x=0,\,y=0}$ = 1 and its image sources at $Z_{x=0,\,y=2nL}$ = 1. This Green's function solution can be treated as the solution of Eq. (11) excited by a Dirac Delta function $\delta\left(x=0,y=0,t=0\right)$, which is used to describe the response to strong external perturbations for the mixture fraction field. Consequently the steady state solution of mixture fraction field Z with a constant release source $Z_{x=0,\,y=0}$ = 1 can be obtained by the temporal convolution of the constant source strength function $I(t)$ and $S_Z(x, y, t)$.

$$\overline{Z}(x,y)=\int_0^{\infty} I\left(t-\zeta\right)S_Z\left(x,y,\zeta\right)d\zeta = I\int_0^{\infty} S_Z\left(x,y,\zeta\right)d\zeta \tag{13}$$

where ζ is the temporal convolution parameter. The constant source strength function

I(t) depends on the boundary condition $Z_{x=0,\,y=0} = 1$, and then the mean mixture fraction field can be obtained from Eq. (13).

Once the mixture fraction field is determined, temperature of the nonpremixed flames can be described by the mixture fraction field. Burke and Schumann flame model is used to describe the relationship between temperature and mixture fraction to simplify the expressions. Therefore temperature can be finally inferred from the distribution of mixture fraction field,

$$\begin{aligned} T(Z) &= T_a + \frac{T_{st} - T_a}{Z_{st}} Z, && Z \le Z_{st} \\ T(Z) &= T_f + \frac{T_f - T_{st}}{1 - Z_{st}} (1 - Z), && Z \ge Z_{st} \end{aligned} \tag{14}$$

where T_f, T_a and T_{st} are temperatures of fuel, air and the stoichiometric flame, respectively. The temperature and mixture fraction solutions are derived from Green's function solution with assumptions similar to those of Burke and Schumann flames. In the following section of results and discussions, the generation and evolution of hot spots (temperature fluctuations) from the theoretical approaches are investigated.

As afore-mentioned, experimental measurements, numerical simulations and theoretical analyses are carried out in this study to investigate the instabilities of nonpremixed flames. The numerical simulations and theoretical analyses are constructed based on many simplified assumptions. Although the numerical simulations were performed in a simplified axisymmetric configuration for an affordable computational cost, they can still complement the experiments and theoretical analyses, where comparisons can be used to identify deficiencies of the methods and to more effectively achieve a deeper physical understanding. To investigate the effects of buoyancy and different external perturbations on the vortex dynamics and instabilities of nonpremixed flames, five cases are performed for reacting plumes of the nonpremixed flame, as shown in Table 1.

Table 1 The computational cases for the parametric study

Case	A	B	C	D	E
perturbation	0	0	20 Hz	30 Hz	40 Hz
buoyancy	0	√	√	√	√

3 Results and discussions

In order to isolate the buoyancy effect from the instability induced by strong external perturbations, numerical results discussed here include five cases, i.e. case A: non-buoyant and undisturbed case; and four buoyant cases: case B: no external perturbation; case C: 20 Hz perturbation; case D: 30 Hz perturbation; case E: 40 Hz perturbation. Three of them (cases C, D, E) correspond to the cases investigated by experiments and theoretical analyses. Experimental, theoretical and computational results are discussed in the following sub-sections.

The instantaneous reaction rate contours of undisturbed cases A, B from numerical simulations at t = 15 are shown in Fig. 4. The effect of buoyancy in reacting plumes can be seen clearly. Chemical reaction occurs when the mixing between fuel and air takes place. For the non-buoyant case chemical reaction occurs in the near-field, and there is no vortical structure, as shown in case A. The prominent feature in case B, however, is the development of outer vortical structures which is responsible for the phenomenon of flame flickering. The motion of outer coherent vortices induces flame stretch at different locations, and then the upward convective motion of flame bulge results in the flame flickering. The interaction between the vortices and the flame surface creates the locally stretched and compressed flamelets. Flame instability is developed in the shear layer originating from the nozzle lip in the presence of buoyancy which rolls up into coherent structures. These structures can merge as they are convected downstream by the streamwise mean flow. In all these buoyant cases B-E in Fig. 5, the outer vortical structures are obvious, which indicate that buoyancy is the prominent factor for flow instabilities associated with flame flickering.

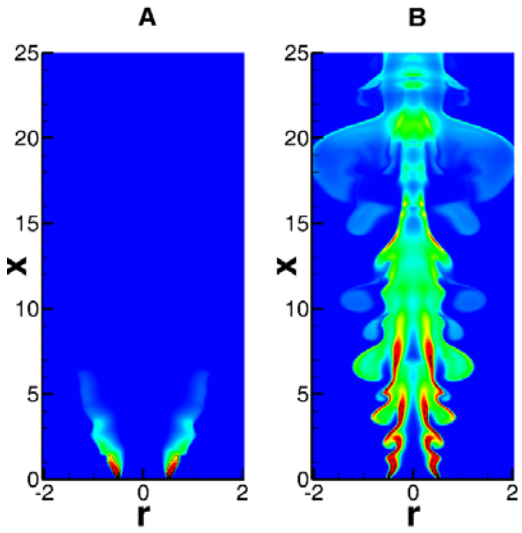

Fig. 4 Reaction rate contours of the undisturbed cases A, B from numerical simulations at t = 15

The parametric study by varying the perturbation frequency is conducted to gain insight into the influence of strong external perturbations and shear layer forcing on the flame dynamics. Fig. 5 shows the instantaneous reaction rate contours of four buoyant cases B-E at t = 15, where the effect of different perturbations on the reacting plumes can be observed from the comparisons. The flame surface can be defined as a thin front where combustion takes place strongly and higher reaction rates exist. The contours shown in black lines in Fig. 5 are the higher reaction rate levels in the flow field, which represent the flame surface. It can be seen that the flame flickering associated with buoyancy is affected by the strong external perturbations, and the coherent structures are disturbed obviously for the cases with external perturbations. It is noted that the nonpremixed flame surface splits eventually at the downstream flow field due to different forced perturbations in cases C-E. The flame surface splits into two parts when perturbations are forced at the inlet boundary. The first part is still attached to the fuel inlet and the other part is located at the downstream flow field. Moreover, the locations of two split flame surfaces are found to be different for cases with different forcing frequencies.

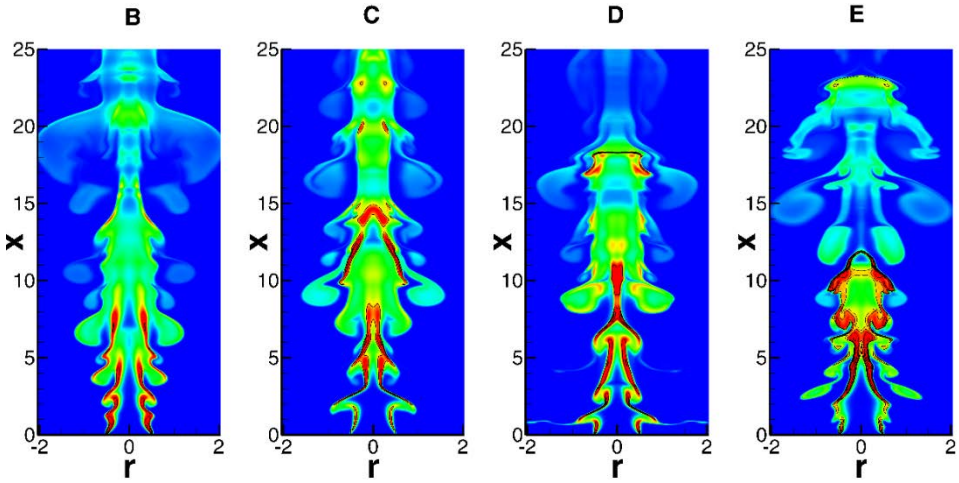

Fig. 5 Reaction rate contours of buoyant cases B-E from numerical simulations at t = 15

Experimental results of the nonpremixed flames are obtained based on high-speed photography in Fig. 6. Strong external perturbations are imposed on the upstream locations of the reacting plumes by two loudspeakers in order to trigger the unstable mode of flames. It can be found that these flames forced by 20 Hz, 30 Hz, 40 Hz perturbations can split into two different combustion regions. One region remains attached to the burner and constitutes the main flame, while the split one detaches from the flame tip, forming a pocket of hot gas surrounded by a flame that travels along the downstream. This can be identified as flame pinch-off. Consequently, flame instability is intensified by the external perturbations. Besides, it is found that flame pinch-off could occur in a short time at the low frequency perturbations especially for the case of 20 Hz perturbation. Accordingly the low-pass characteristic of forced reacting plumes is manifested in the experiments. It is worth noting that the results in Fig. 6 are from the measurements of the light intensity in different parts of the nonpremixed flames, while Fig. 5 shows numerical results based on a simplified one-step global chemistry of the nonpremixed combustion. In general, the experimental results in Fig. 6 are consistent with the results of numerical simulations shown above in terms of flame dynamics such as the periodic behaviour and the flame pinch-off phenomenon.

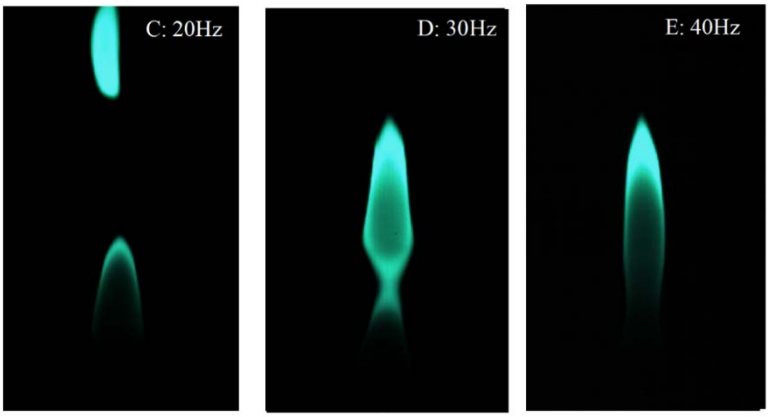

Fig. 6 High-speed photograph of the nonpremixed flame from the experiments

As shown in Fig. 7, the generation of hot spots (temperature fluctuations) is obtained based on theoretical approaches, which is derived from Green's function solution with some assumptions similar to those of classical Burke and Schumann diffusion flames. Temperature fluctuations and flame surface described with a black curve are illustrated in consistence with flame pinch-off studied in the experimental and numerical results. Compared with Fig. 5 and Fig. 6, it can be easily observed that flame surface breaks in forced reacting plumes, and there are two flame fronts formed in the hot spots. In addition, a backward movement of the position for the second flame front is manifested with the increasing forced perturbations, which indicates that the nonpremixed forced flames with low frequency perturbations tend to develop the convective instability in a short time. The low-pass characteristics are also verified by the generation of hot spots in theoretical analyses.

For the forced reacting plumes, flame pinch-off occurs under a specific condition, which is not a common phenomenon. When mixture fraction Z meets the requirements of the following equation simultaneously at $r = 0$, flame surface is supposed to split into two parts (Carpio et al., 2012).

$$\begin{aligned} Z - Z_{st} &= 0 \\ \frac{\partial}{\partial x}\left(Z - Z_{st}\right) &= 0 \\ \frac{\partial}{\partial t}\left(Z - Z_{st}\right) &= 0 \end{aligned} \tag{15}$$

Eq. (15) is the mathematical representation for the break of stoichiometric surface that

generates two combustion regions. The break of stoichiometric surface acts as a dividing line for fuel-rich zone and fuel-lean area. One surface remains attached to the burner and constitutes the main flame which corresponds to the fuel-rich zone at the inner stoichiometric surface, while another detaches from the tip of the flame, forming a pocket of hot gas surrounded by a flame that travels along the downstream where fuel is lean. From a physical standpoint, flame pinch-off is a local flame extinction induced by the effective entrainment of air in the central region of the jet that leaves no fuel remaining to be burnt. Flame pinch-off is affected by the strong forced perturbations introduced at the jet nozzle exit, and the low-pass characteristic is observed in the forced reacting plumes. It is evident that the nonpremixed reacting plume system is sensitive to the low frequency perturbations. The convective instability of reacting plumes characterized by the low-pass characteristic can be seen due to the effect of strong external perturbations.

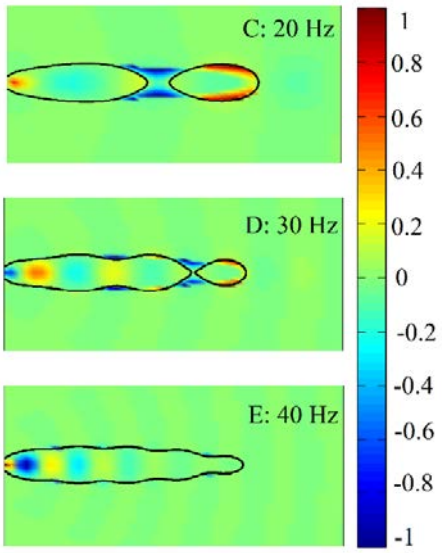

Fig. 7 Temperature fluctuation, flame surface of cases C, D and E from the theoretical analyses

In order to understand the generation and evolution process of the two flame fronts, the periodical behaviors of nonpremixed flames are exhibited in Fig. 8. The evolution of hot spots from the theoretical analyses, high-speed photographs and Schlieren of methane-air coflow flames obtained from the experiments and reaction rate contours calculated from numerical simulations in one period of time with 30 Hz forced external perturbation are demonstrated respectively. The red lines in Fig. 8 are shown to indicate

the location where the flames begin to split. Considering that one period of time is equally divided into five parts, the non-dimensional time interval of the images is 0.83. It can be observed from the red lines that temperature and reaction rate fields oscillate with the same frequency, and the oscillating frequency of the forced reacting plume is 30 Hz. The fluctuations are convected with the velocity of the bulk flow. The periodic oscillations in the experimental results are consistent with those shown in theoretical analyses and numerical simulations. In the nonpremixed combustion system, temperature varies periodically in response to the strong perturbations at the source. Temperature fluctuations give rise to pressure oscillations, leading to the low frequency combustion oscillation (Cumpsty and Marble, 1977). The hot spots can be described as

$$\frac{T'}{T} = \frac{s'}{c_p} + (\gamma - 1)\frac{p'}{\gamma p} \tag{16}$$

Here the first term on the right-hand side of Eq. (16) stands for the entropy perturbations and the second term represents the isentropic temperature change caused by pressure perturbations. In the combustion zone, two distinct regions can be found. The location of stoichiometric surface acts as a dividing line for fuel-rich zone and fuel-lean region. In the region near the fuel source fuel is rich, an increase of mixture fraction leads to a decrease of temperature and develops the first flame front of forced reacting plumes in Fig. 8. However, an increase of mixture fraction results in a positive temperature fluctuation in the outer stoichiometric surface. The location of the second flame front corresponds to the position where the maximum temperature fluctuation is reached. The magnitude of temperature gradually decays as mixture fraction wave tide propagates towards downstream. Consequently there are two combustion regions in the forced reacting plumes. Hence the flame surface can split into two parts and the split part moves downstream and gradually decays due to the diffusion process. Furthermore, these behaviors of flame pinch-off are found to be periodically formed.

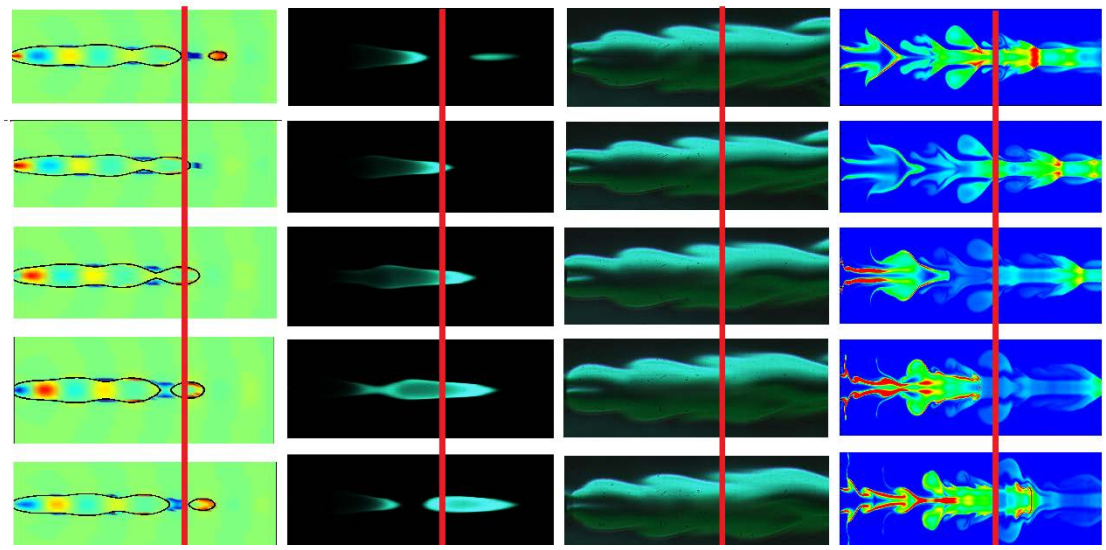

(a) (b) (c) (d)

Fig. 8 Temperature fluctuation and flame surface from the theoretical analyses (a), high-speed photograph of the flame from the experiments (b), Schlieren of the flame from the experiments (c) and reaction rate contours from numerical simulations (d)

The vortical structure plays a key role in understanding the instabilities of nonpremixed flames. As mentioned above, buoyancy is responsible for the flow instabilities associated with flame flickering and coherent structures. Flickering of the nonpremixed buoyant reacting plumes is a common phenomenon for the global instability. To isolate the instability induced by external perturbations, buoyancy alone triggers the unstable mode in case B. The coherent outer vortices are sequentially developed in the near-field for the nonpremixed flames. Such a well-organized structure suggests that buoyancy plays an important role in the development of absolute instability associated with flame flickering. In addition, there is a tendency of vortex merging (Cerretelli and Williamson, 2003) in the downstream of the flow field, while the vortices remain coherent in the upstream, as shown in Fig. 9. Vortex merging of neighbouring coherent vortices is an important phenomenon as they travel downstream, especially for case B without the influence of forced external perturbations. The merging of vortical structures is predominant in the growth of larger structures, and two co-rotating vortices of like-sign can merge to form a single vortex. During the vortex merging, the two centroids of co-rotating vortices are readily pushed towards each other

by the local velocity field.

In the four buoyant cases B-E, the outer vortices dominate the flow field, while counter rotating vortices are also found in Fig. 9. The counter rotating vortices exist at the plume base due to entrainment, particularly for the cases of low frequency perturbations. The effect of entrainment can be observed clearly in cases C, D and E, where flame pinch-off takes place. Flame pinch-off is induced by the effective entrainment of air in the central region of methane jet flame that leaves no fuel remaining to be burnt. Two flame surfaces spread downstream as fuel and air mix and burn at the stoichiometric surface. Consequently the convective instability associated with the effect of external perturbations of forced plumes is intensified with strong mixing and entrainment. Since the jet shear layer of burnt gases exhibits an inflexional velocity profile for the strong mixing and entrainment, the nonpremixed flame is unstable in the sense of convective instability. In addition, the vortical structure indicates a strong effect of flame stretch and compression. The interactions of vortices and flamelets including the squeezed and bulged effects are attributed to the local extinctions. Therefore two flame fronts are formed when buoyancy instability is coupled with the convective instability, and their interaction between the instabilities is linked with the low-pass characteristic of nonpremixed flames.

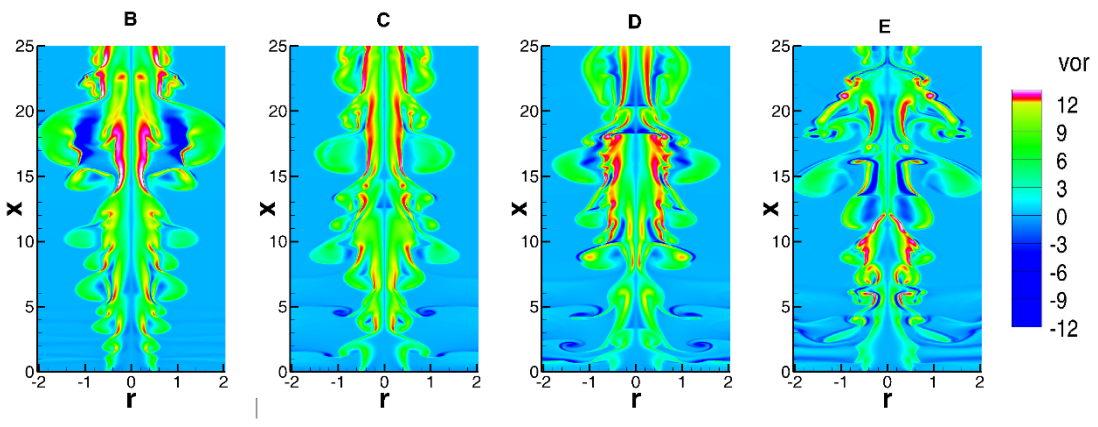

Fig. 9 Vortices contours of the axisymmetric buoyant thermal plumes from numerical simulations at t = 15, cases B-E

The history of centerline velocity at x = 1 and the corresponding Fourier spectra for the reacting plumes are shown in Fig. 10. The periodic behaviour is apparently seen

from the history of centerline velocity, particularly for the undisturbed case B. Fourier spectrum calculations provide the frequencies of flame oscillations. It can be observed that the dominant frequency corresponding to the undisturbed case B is located at a non-dimensional value at about 0.33. Considering a reference length scale of 4.5 mm and reference velocity 0.558 m/s, this corresponds to a dimensional value about 40 Hz. For the undisturbed buoyant case B, there is only one high peak at 0.33 in the Fourier spectrum which is associated with the buoyancy effect. Once the unstable mode has been triggered into growth in an absolute buoyancy-driven instability, the reacting plume tends to oscillate in a self-sustaining manner.

It can be seen that the dominant frequencies corresponding to the disturbed cases C and D are similar to that in the undisturbed buoyant case B, with a non-dimensional value at about 0.33, corresponding to 40 Hz forced frequency. Therefore, buoyancy still plays an important role in the determination of the frequency spectra, albeit with the high level of disturbance used. In addition, it is noted that there are two peaks of frequencies in cases C, D and E. For the three disturbed buoyant cases, another peak ahead of dominant frequency peak is shown in the Fourier spectra. The second peak for case C is located at a non-dimensional frequency 0.15 (about 20 Hz), which is linked with the forced 20Hz perturbation at the origin. The low peak is related to the forced frequency at the jet nozzle exit, while the high peaks are associated with the convection speed of vortical structures in the flow field. The convection speed of vortical structures not only depends on the buoyancy effect, but also depends on the mixing process, which is found to be amplified in forced reacting plumes. Accordingly, the amplitudes for forced perturbation cases are all larger than those for the undisturbed case. It is worth pointing out that when the dominant frequency of forced reacting plumes approaches that of the undisturbed case more closely, flame pinch-off occurs more easily. This is one proof that the flame instability is amplified by the low frequency oscillation coupled with the buoyancy effect.

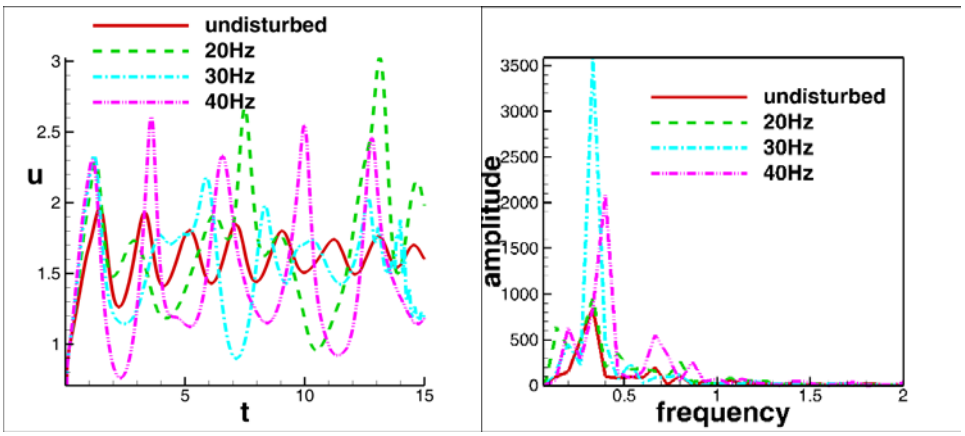

(a) Centerline velocity history (b) Fourier spectra

Fig. 10 History of the centerline velocity at x = 1 (a) and the Fourier spectra (b) for the axisymmetric reacting plumes, cases B-E

Since flame pinch-off is effectively triggered by a strong entrainment of air in the central region, the flame front splits apparently at the downstream locations. Besides, it is found that the forced reacting plumes of low frequency perturbations are easier to split and develop the flame instability, referred to as the convective instability, while buoyancy instability is found to be an intrinsic flow instability which is of an absolute unstable nature. These two types of instabilities differ markedly in their susceptibility to external sequential disturbances. When the unstable mode has been triggered into a growth in an absolute buoyancy-driven instability, the reacting plume tends to oscillate in the self-sustaining manner. On the other hand, a convectively unstable plume is susceptible to subsequent strong perturbations at the nozzle exit, especially for the low frequency perturbations. Buoyancy instability coupled with convective instability has a strong effect on flame stretch and eventually leads to the break of nonpremixed flames. With the combination of experimental results, numerical simulations and theoretical analyses, it is evident that nonpremixed reacting plume system is more sensitive to the low frequency perturbations, and convective instability of reacting plumes is amplified clearly due to the effect of forced external perturbations. However, the flow turbulent behaviours such as the asymmetric and irregular vortical structures are not fully developed due to the limitations of two-dimensional nature of the axisymmetric simulation, which can only be fully captured in a three-dimensional simulation. It is

worth noting that the instabilities and their interaction for reacting plumes in this study are manifested clearly. Despite the fact that there are some limitations in the two-dimensional axisymmetric direct numerical simulations, the axisymmetric cases are considered to be sufficient to investigate these near-field instabilities instead of fully three-dimensional simulations for a general understanding of the dynamics of the turbulent reacting flows. Currently three-dimensional numerical simulations are being carried out to allow for quantitative comparison with experimental results.

4 Conclusions

A comparative and integrated study using all three approaches: experiments, theoretical analyses and numerical simulations is performed to investigate the flow instabilities and their interactions for nonpremixed methane-air flames. Theoretical analyses are derived from the single transport equation for mixture fraction with a series of assumptions, and results are still in good agreement with the analyses of experiments and numerical simulations. It is confirmed that buoyancy instability is an intrinsic flow instability which is of an absolute unstable nature, while convective instability is intensified because of the strong external perturbation effects. The outer vortices due to buoyancy dominate the flow field, and some counter rotating vortices exist at the plume base due to entrainment. Besides, flame pinch-off occurs further downstream due to the interaction between buoyancy instability and convective instability. The break of stoichiometric surface acts as a dividing line for the fuel-rich zone corresponding to the flame front attached to the burner and fuel-lean area for another flame front spreading downstream. It is noted that the nonpremixed flame system has a low-pass characteristic, which is sensitive to the low frequency perturbations. In general, the predictions from the experimental, theoretical and computational approaches are in qualitative agreements with each other for the near-field dynamics of the reacting plumes of the nonpremixed flames.

Acknowledgements

This research was supported by the National Natural Science Foundation of China (Grants No. 51376107).

Nomenclatures

A	amplitude
c_p	heat capacity
Da	Damk**ö**hler number
e	internal energy
f_0	frequency
Fr	Froude number
g	gravity
Ma	Mach number
p	pressure
Pe	Péclet number
Pr	Prandtl number
q_h	rate of heat release
Re	Reynolds number
s	entropy
Sc	Schmidt number
T	temperature
t	time
u	axial velocity
v	radial velocity

w_Y	chemistry reaction rate
Y_i	mass fraction of species
Z	mixture fraction
γ	ratio of specific heats
μ	viscosity
ρ	density
ζ	temporal convolution parameter

Superscripts

-	averaged quantity
$'$	perturbation quantity
*	dimensional quantity

Subscripts

a	air
f	fuel
0	inlet

References

Balasubramanian, K., Sujith, R., 2008. Non-normality and nonlinearity in combustion-acoustic interaction in diffusion flames. J. Fluid Mech. 594, 29-57.

Buckmaster, J., Peters, N., 1988. The infinite candle and its stability-a paradigm for flickering diffusion flames. Symp. (Int.) Combust. 1829-1836.

Carpio, J., Sánchez-Sanzb, M., Fernández-Tarrazoc, E., 2012. Pinch-off in forced and non-forced, buoyant laminar jet diffusion flames. Combust. Flame 159, 161-169.

Cerretelli, C., Williamson, C., 2003. The physical mechanism for vortex merging. J. Fluid Mech. 475, 41-77.

Chamberlin, D., Rose, A., 1928. The flicker of luminous flames. Ind. Eng. Chem. 20,

1013-1016.

Cumpsty, N., Marble, F., 1977. The interaction of entropy fluctuations with turbine blade rows; a mechanism of turbojet engine noise. Proc. R. Soc. London, Ser. A. 357, 323-344.

Doom, J., Mahesh, K., 2009. Direct numerical simulation of auto-ignition of a hydrogen vortex ring reacting with hot air. Combust. Flame 156, 813-825.

Eickhoff, H., 1982. Instability and coherent structures in jet flames. Recent Contributions to Fluid Mechanics. Springer.

Goss, L.P., Katta, V.R., Roquemore, W.M., 1994. Simulation of vortical structures in a jet diffusion flame. Int. J. Numer. Methods Heat Fluid Flow. 4, 413-424.

Gotoda, H., Ueda, T., Shepherd, I.G., Cheng, R.K., 2007. Flame flickering frequency on a rotating Bunsen burner. Chem. Eng. Sci. 62, 1753-1759.

Grout, R.W., Gruber, A., Kolla, H., Bremer, P.-T., Bennett, J.C., Gyulassy, A., Chen, J.H., 2012. A direct numerical simulation study of turbulence and flame structure in transverse jets analysed in jet-trajectory based coordinates. J. Fluid Mech. 706, 351-383.

Huerre, P., Monkewitz, P., 1985. Absolute and convective instabilities in free shear layers. J. Fluid Mech. 159, 151-168.

Jiang, X., 2010. Numerical studies of vortex shedding in forced oscillatory nonpremixed flames. IOP Conf. Ser.: Mater. Sci. Eng. 10, 012030.

Jiang, X., Luo, K.H., 2000a. Combustion-induced buoyancy effects of an axisymmetric reactive plume. Proc. Combust. Inst. 28, 1989-1995.

Jiang, X., Luo, K.H., 2000b. Spatial direct numerical simulation of the large vortical structures in forced plumes. Flow Turbul. Combust. 64, 43-69.

Juniper, M.P., Li, L.K.B., Nichols, J.W., 2009. Forcing of self-excited round jet diffusion flames. Proc. Combust. Inst. 32, 1191-1198.

Katta, V.R., Goss, L.P. Roquemore, W.M., 1994. Numerical investigations of transitional H_2/N_2 jet diffusion flames. AIAA J. 32, 84-94.

Lele, S.K., 1992. Compact finite difference schemes with spectral-like resolution. J. Comput. Phys. 103, 16-42.

Lieuwen, T.C., 2012. Unsteady combustor physics. Cambridge University Press.

Magina, N., Shin, D.H., Acharya, V., Lieuwen, T., 2013. Response of nonpremixed flames to bulk flow perturbations. Proc. Combust. Inst. 34, 963-971.

Poinsot, T., Veynante, D., 2005. Theoretical and numerical combustion (2nd ed). R.T. Edwards, Inc.

Poinsot, T.J., Lele, S.K., 1992. Boundary conditions for direct simulations of compressible viscous flows. J. Comput. Phys. 101, 104-129.

Roquemore, W.M., Chen, L.D., Goss, L.P., Lynn, W.F., 1989. The structure of jet diffusion flames. Turbulent Reactive Flows. Lecture Notes in Engineering 40, 49-63. Springer.

Savas, O., Gollahalli, S., 1986. Flow structure in near-nozzle region of gas jet flames. AIAA J. 24, 1137-1140.

Stakgold, I., Holst, M. J., 2011. Green's functions and boundary value problems. John Wiley & Sons.

Tyagi, M., Chakravarthy, S.R., Sujithc, R.I., 2007. Unsteady combustion response of a ducted nonpremixed flame and acoustic coupling. Combust. Theor. Model. 11, 205-226.

Wang, Q., Darabkhani, H.G., Chen, L., Zhang, Y., 2012. Vortex dynamics and structures of methane/air jet diffusion flames with air coflow. Exp. Therm. Fluid Sci. 37, 84-90.

Wang, Q., Huang, H.W., Tang, H.J., Zhu, M., Zhang, Y., 2013. Nonlinear response of buoyant diffusion flame under acoustic excitation. Fuel 103, 364–372.

Williamson, J., 1980. Low-storage runge-kutta schemes. J. Comput. Phys. 35, 48-56.

Yao, Z., Zhu, M., 2012. A distributed transfer function for nonpremixed combustion oscillations. Combust. Sci. Technol. 184, 767-790.

Yule, A., Chigier, N.A., Ralph, S., Boulderstone, R., Venturag, J., 1981. Combustion-transition interaction in a jet flame. AIAA J. 19, 752-760.

Zhu, M., Dowling, A.P., Bray, K.N.C., 2005. Transfer function calculations for aeroengine combustion oscillations. J. Eng. Gas Turbines Power 127, 18-26.